

Low-Dose Studies of Bystander Cell Killing with Targeted Soft X Rays

G. Schettino,^{a,1} M. Folkard,^a K. M. Prise,^a B. Vojnovic,^a K. D. Held^b and B. D. Michael^a

^a Gray Cancer Institute, P.O. Box 100, Mount Vernon Hospital, Northwood, Middlesex, HA6 2JR, United Kingdom; and ^b Department of Radiation Oncology, Massachusetts General Hospital, Harvard Medical School, Boston, Massachusetts

Schettino, G., Folkard, M., Prise, K. M., Vojnovic, B., Held, K. D. and Michael, B. D. Low-Dose Studies of Bystander Cell Killing with Targeted Soft X Rays. *Radiat. Res.* 160, 505–511 (2003).

The Gray Cancer Institute ultrasoft X-ray microprobe was used to quantify the bystander response of individual V79 cells exposed to a focused carbon K-shell (278 eV) X-ray beam. The ultrasoft X-ray microprobe is designed to precisely assess the biological response of individual cells irradiated *in vitro* with a very fine beam of low-energy photons. Characteristic C_K X rays are generated by a focused beam of 10 keV electrons striking a graphite target. Circular diffraction gratings (i.e. zone plates) are then employed to focus the X-ray beam into a spot with a radius of 0.25 μm at the sample position. Using this microbeam technology, the correlation between the irradiated cells and their nonirradiated neighbors can be examined critically. The survival response of V79 cells irradiated with a C_K X-ray beam was measured in the 0–2-Gy dose range. The response when all cells were irradiated was compared to that obtained when only a single cell was exposed. The cell survival data exhibit a linear-quadratic response when all cells were targeted (with evidence for hypersensitivity at low doses). When only a single cell was targeted within the population, 10% cell killing was measured. In contrast to the binary bystander behavior reported by many other investigations, the effect detected was initially dependent on dose (<200 mGy) and then reached a plateau (>200 mGy). In the low-dose region (<200 mGy), the response after irradiation of a single cell was not significantly different from that when all cells were exposed to radiation. Damaged cells were distributed uniformly over the area of the dish scanned ($\sim 25 \text{ mm}^2$). However, critical analysis of the distance of the damaged, unirradiated cells from other damaged cells revealed the presence of clusters of damaged cells produced under bystander conditions. © 2003 by Radiation Research Society

INTRODUCTION

Current studies of radiation effects in cellular systems have found a range of responses which predominate at low doses and low dose rates (1–3). Bystander responses, where

unirradiated cells neighboring those which have been targeted are seen to respond, have attracted considerable interest. An important question is the efficiency of low-LET radiations at inducing bystander responses and the mechanisms and targets involved. For conventional low-LET radiations, a significant part of the effect is due to the several hundreds of electron volts deposited at the terminal end of each electron track. A useful model for examining these terminal electron tracks is studies with ultrasoft X rays (4). The recent technological developments in the control and delivery of radiation combined with the increasing improvements in assays of individual cells have generated a new wave of interest in single-cell microirradiation techniques for radiobiological purposes. Modern microbeams offer the opportunity to deliver precise doses to preselected individual cells or parts of cells *in vitro*. They also allow precise control of the distribution of dose within individual cells and the number and position of irradiated cells within the entire sample. The most advanced microbeams presently used in radiobiology² (5, 6) are able to irradiate single cells with charged-particle beams collimated or focused down to micrometer size. The ultrasoft X-ray microprobe (7, 8) is the first microbeam facility to use X rays for radiobiological purposes. The microprobe facility has unique characteristics that make it particularly suitable to address a number of important questions relevant to spatial aspects of the interaction of ionizing radiation with tissue. As well as allowing fast irradiation of individual cells and the revisiting of a large number of samples, the microprobe can produce a finer probe than is achievable using our charged-particle microbeam. Using the microprobe, focused spots significantly less than 1 μm in diameter are possible. Moreover, the energy is not dispersed by scattering, and the range of the secondary electrons produced by the absorption of C_K photons is less than 10 nm. Therefore, a localized energy deposition is achieved, allowing researchers to specifically probe the radiobiological relevance of subcellular compartments.

The aim of this study was to determine the effectiveness of focused C_K photons in cell killing under conditions in

¹ Address for correspondence: Gray Cancer Institute, Mount Vernon Hospital, Northwood, Middlesex, UK, HA6 2JR; e-mail: Schettino@gci.ac.uk.

² G. Randers-Pehrson, Operating characteristics of the Columbia alpha-particle microbeam, Particle microbeam workshop, 1, 1994.

which every cell or only one cell within a population was targeted.

MATERIALS AND METHODS

Cell Culture

V79-379A Chinese hamster cells were cultured in T-25 flasks and incubated at 37°C in an atmosphere of 95% air/5% CO₂. During the incubation period, cells were grown in filtered Eagle's Complete Minimal Essential Medium (CMEM) containing 10% fetal calf serum, penicillin (100 IU/ml) and streptomycin (100 µg/ml). On the morning of the experiments, cells were detached from the flask by minimal treatment with trypsin (0.25% w/v in phosphate-buffered saline, PBS) and diluted to obtain a single cell suspension. Cells were seeded into specially designed dishes with a 0.9-µm-thick Mylar base on which cells attach. After trypsinization and dilution, the seeded cells normally contained $5.49 \pm 0.97\%$ clusters of cells (mainly newly divided doublets) with the rest being single cells. The clustered cells were marked individually during the automatic cell finding process and excluded from the survival analysis. A suitable spacing between cells was achieved by limiting the concentration of cells plated to about 9×10^3 cells/dish (~ 9.1 cm²). Since that the attaching efficiency of V79 cells on Mylar substrate after 4 h (i.e. time between cell plating and irradiation) is about 80%, this led to a final average concentration of about 160 cells per experimental region on which the survival was assessed. The experimental region corresponded to a 5×5 -mm² area situated in the middle of the culture dish. Cell nuclei were stained with Hoechst 33258 at a concentration of 1 µM about 1 h prior to the irradiation according to a tested nontoxic protocol (8). The CMEM containing the dye was removed before the start of the experiment, and after a wash with fresh CMEM, the cells were incubated in Hepes (20 nM)-buffered CMEM (approximately 2 ml) for the irradiation. The Hepes solution guaranteed a stable pH value and suitable biological conditions for the cells during the time they were exposed in air for the irradiation (~ 30 min). After the irradiation, cells were reincubated for 3 days in CMEM.

Microprobe Experimental Procedure

A series of initialization and registration routines must be performed before the beginning of the biological experiments to assure the required precision and accuracy. These routines involve achieving the optimum running conditions for the X-ray source, necessary to obtain a nearly monochromatic C_K X-ray beam at a stable dose rate, the alignment of the X-ray focusing elements, and the registration of the micropositioning stage. As reported previously (9), the X-ray source has been well characterized, and stable operating conditions for a nearly monochromatic C_K X-ray beam are readily achieved.

The correct alignment of the focusing elements (i.e. zone plate and order selecting aperture, OSA) is of critical importance for the correct irradiation of the samples. First, a 200-µm-radius zone plate must be positioned above the center of a 500×500 -µm vacuum window such that it is illuminated by the emerging radiation. This alignment is performed using a 10× objective, and it is relatively straightforward since the accuracy of alignment required is not critical. Much more critical is the position of the OSA, a small pinhole (6.25 µm radius) close to the first-order focus. The role of the OSA is to reduce the contribution of the unfocused radiation to the samples and also to make the focal spot easy to locate during the irradiation procedure. The OSA is positioned at a precise distance from the zone plate, only a few micrometers shorter than the radiation focus length. This is the point where the X rays are focused, which can be calculated knowing the zone plate characteristics and the wavelength of the radiation used. The motorized objective (10×) is again used to accurately set this distance by focusing first on the zone plate, then raising the objective by the desired amount, and finally positioning the OSA at the objective focus. The X-Y position of the OSA is set by

accurately moving the OSA while monitoring the radiation that exits from it with an X-ray detector (proportional chamber). When the X-ray focus is centered with the OSA, a sharp increase in the C_K X-ray dose rate is observed. For this alignment, the OSA is coupled to the motorized micropositioning stage normally used to support and position the culture dish during the experiment. Once the alignment is achieved, the OSA is decoupled from the stage, leaving it free for the cell dish, while a magnetic coupling arrangement keeps the OSA in position (8). For the experiments described in this paper, the whole cell nucleus was considered as the target. Using well established image analysis and micropositioning techniques (8), cell nuclei can be aligned with the OSA with an absolute accuracy of ± 3 µm that assures a successful irradiation considering the size of the designated target (~ 5 µm radius). However, when more accurate targeting resolution is required, the exact position of the X-ray focus spot can be located by scanning a sharp edge mask across the OSA while monitoring the changes in X-ray dose rate. The position of the mask at the point at which it starts to obstruct the X-ray beam is taken as an indication of the X-ray focus position. This technique is also used to measure the size of the X-ray focus spot (8). This alignment procedure is done only occasionally as required. If the alignment is preserved, only the X-ray dose rate is checked with the detector before the biological experiments for dosimetric purposes. Finally, a registration procedure for the stage and the motorized objective must be carried out to establish the relationship between the microscope image and the stage coordinate system.

Once all the initialization and registration routines are completed, the dish is placed on the stage for the start of the biological experiment. The first operation (*scanning*) consists of the acquisition of 80 overlapping frames (with a 20× water immersion objective and epifluorescence illumination) to result in a complete map of all the fluorescent objects present in a preselected 5×5 -mm² region. In the second step (*revisiting*), all the objects found are revisited individually and, at this stage, the operator has the opportunity to classify the objects as single cells, clusters of cells, and debris or other false signals. The coordinates of all the objects found and the operator classifications are then stored in a file. The dish is then placed in the irradiation position; i.e., the stage is set to an appropriate height such that the cell nuclei are in the X-ray focal plane. This is achieved by adjusting the objective until the image of the OSA is in focus and subsequently moving the cells into the objective focus. Having initially positioned the higher part of the OSA just few micrometers below the X-ray focus, this procedure will assure that the X-ray focus will lie inside the cell nuclei. The nucleus thickness (~ 8 µm) and the depth of the X-ray focus (± 6 µm) give a relatively comfortable range of confidence. The third and final step (*irradiation*) starts with the location of the OSA. The OSA is viewed through the Mylar film and its center is marked with a crosshair. The X-ray source is then switched on, and once the X-ray source has reached the required running conditions, the irradiation procedure takes place. This consists of automatically recalling the coordinates of the single cell(s) that has to be irradiated, aligning it with the crosshair, and exposing each sample to the X-ray beam for a set length of time. The exposure time is established from the dosimetric measurements performed before the start of the experiment and the dose that had been selected for that particular experiment. It takes less than 10 min to scan a 25-mm² area of the dish and to locate and classify about 200 targets, while the irradiation time depends strongly on the dose rate, on the dose delivered to each sample, and on the number of samples to be irradiated. The control dish is subjected to a similar UV-radiation exposure and scanning procedure, but no X-ray dose is delivered to the cells. After an incubation period of 3 days, the dishes are replaced on the stage, and the coordinates of all the samples are revisited to analyze the fate of each cell individually. The colonies are viewed again under UV illumination after having been restained with Hoechst. Using this individual revisiting technique and a 20× objective, the fraction of the cells surviving is assessed precisely by adopting the classical criterion of 50 cells per colony. Although the incubation period (3 days) is considerably shorter than that adopted in conventional clonogenic assays for V79 cells (7 days), it has been shown previously (10) that this technique generates

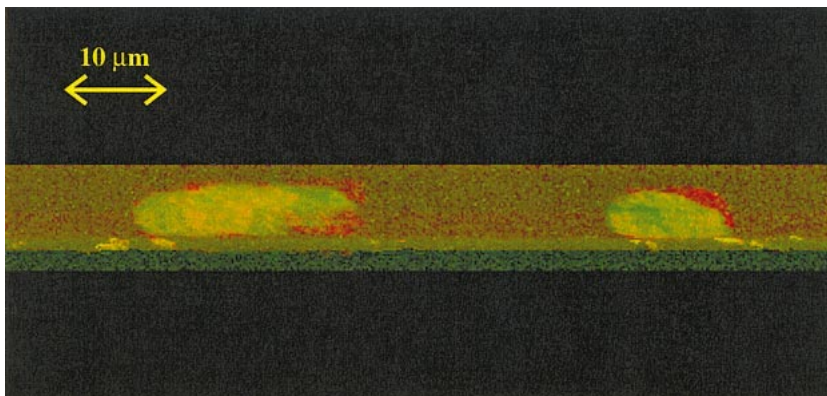


FIG. 1. Vertical section of a confocal image of V79 cells plated on Mylar (3 μm thick) 4 h after seeding. Cell nuclei were stained with 10 μM of Hoechst 33258 for 1 h (green signal) and the cytoplasm with 50 μM of Rhodamine 123 for 15 min (red signal). In the figure, the Mylar film on which the cells are attached is also visible due to the intrinsic fluorescence of Mylar (which has an similar emission wavelength similar to that of Hoechst 33258).

results that are in very good agreement with those using traditional clonogenic procedures.

Dosimetry

The estimation of the dose delivered to each individual sample is based on the measurements of the X-ray dose rate performed using a gas-filled proportional chamber. The detector anode is made by a brass pin with a hemispherical end (~ 0.5 mm radius) positioned in the center of an aluminum chamber kept at 0 V. The inside of the chamber has a hemispherical shape to produce a uniform electric field around the anode. A 0.9- μm -thick Mylar film is used as radiation entrance window above the pin so that the radiation enters the detector parallel to the anode. The chamber is filled with typical detection gas (P10) at a flow rate of ~ 10 ml/s; it is normally operated at an anode voltage of about -1.9 kV. The small size of this detector allows it to be placed directly above the source, replacing the microscope objective during the dosimetric procedure. The detector output is analyzed by a computerized multichannel analyzer to obtain the energy distribution of the photons emerging from the source. This allows us to quantify the C_K X-ray flux separately from the bremsstrahlung component. The detector efficiency for the C_K X rays is dominated mainly by the attenuation in the entrance window (C_K transmission through 0.9 μm Mylar is 65%) since the probability that the photon will be absorbed in the gas volume is $>99\%$. However, the 0.9- μm Mylar film is also used as a substrate for the biological samples, so the C_K X-ray dose rate measured by the detector is therefore similar to that received by the cells during the irradiation. Correction factors must be used to estimate the bremsstrahlung dose rate. The X-ray dose rate is measured before and after each biological experiment, and an agreement within 5% is generally observed providing that the X-ray source has stabilized (normally after ~ 15 min).

Carbon K-shell X rays are attenuated very easily by biological tissues, and the absorbed dose decreases exponentially with the depth in the cell. Assuming that a cell has a composition similar to that of the spleen and a typical density of 1.08 g/cm³, the absorbed dose is reduced by a factor of 2.2 for every 1 μm of cell depth. For traditional irradiation techniques using ultrasoft X rays, the radiobiological effects are generally reported as a function of either the incident dose or the nuclear dose. The incident dose indicates the average amount of energy deposited in the cell divided by its whole mass, while the nuclear dose refers to the amount of energy absorbed only in the cell nucleus. All data shown in this work are reported as a function of the nuclear dose. Almost all the energy deposited by C_K X rays is through photoelectric absorption, and the energy is highly localized since the secondary electrons have a very short range (typically about 7 nm). The nuclear dose was calculated considering the number of photons absorbed by the cell nucleus and dividing the corresponding

energy deposited by the nuclear mass (5.65×10^{-13} kg, assuming a 5- μm -radius sphere with 1.08 g/cm³ density). To calculate the nuclear dose from our measurements of the incident dose, it is of critical importance to know about cell morphology and in particular to measure the thickness of the cytoplasm layer nearest to the source during the irradiation. These measurements were performed using a two-photon microscope based at the Gray Cancer Institute and following the same protocol and time scale used for the microprobe experiments. This ensured that the measurements described the exact morphology of the cells at the time of irradiation. Cells were stained with Hoechst 33258 (10 μM for 1 h) to stain the cell nucleus and Rhodamine 123 (50 μM for 15 min) to stain the mitochondria (i.e. cytoplasm). V79 cells attach easily on a variety of substrates. However, 4 h after seeding, although they are firmly attached to the Mylar film, they still have a spherical shape and are not very well spread (Fig. 1). The results from thickness measurements indicate a cytoplasm gap (Mylar–cell nucleus) of 0.7 ± 0.5 μm and an overall nuclear thickness of 8.0 ± 1.1 μm . About 35% of the total dose delivered to the cell will therefore be absorbed by the cytoplasm, and more than 50% will be concentrated in the first 4 μm inside the nucleus. The bremsstrahlung contribution will be negligible, only 0.05% of the total dose. Moreover, considering the high spatial resolution of the X-ray beam (<0.5 μm focus spot) and the low energy of the secondary electrons produced (7 nm range), it follows that almost all ionizations will be produced within a volume smaller than 1 μm^3 . These figures underline the high localization of energy deposition achieved using the microprobe.

RESULTS

Control Experiments

To obtain a very accurate measurement of survival, we have developed an experimental procedure that allows us to correlate the presence of each surviving colony with its parent. This is achieved by incubating the cells in the same irradiation dish where their coordinates have been stored prior to the irradiation and then revisiting them during the colony scoring. The statistical advantage of such an approach has been discussed previously (9). For this purpose, it is therefore necessary to plate a statistically relevant number of cells, at a density suitable to allow colonies to form and be distinguishable individually. Control experiments are of critical importance in the estimation of the clonogenic assay using the microprobe technique since they will

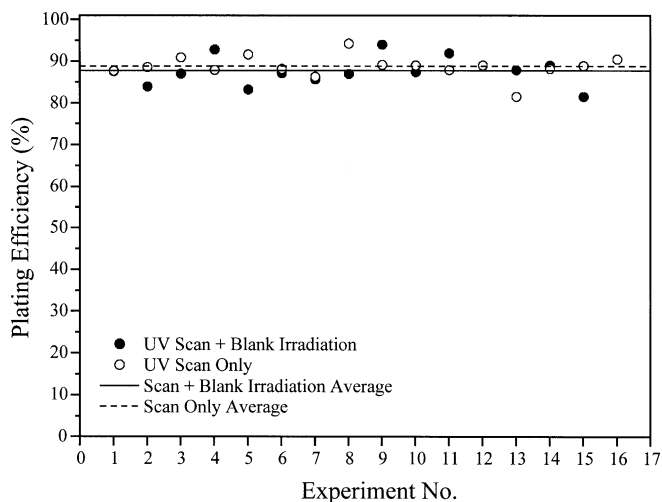


FIG. 2. Plating efficiencies for the control experiments. (●) Cells exposed to a typical UV-light scan followed by irradiation (1 Gy) focused into an empty space (i.e. medium irradiation). (○) Cells exposed to a UV-light scan only; (—) average value for the scan plus blank irradiation; (---) average value for the scan-only experiments.

provide the survival value against which the fraction of surviving cells from the irradiated dishes must be normalized. As reported earlier (9), several factors can influence the clonogenic potential of the cells during a typical microprobe experiment. Other than radiation, fluorescence staining (Hoechst 33258), UV-radiation exposure, intrinsic plating efficiency, and cell stress are the major factors. Preliminary measurements (9) have optimized the staining and scanning protocol to obtain bright cell nuclei clearly identifiable by the automated image analysis system of the facility without producing a significant alteration of the of the clonogenic potential of the cells. The final concentration of Hoechst is kept below $1 \mu\text{M}$ (staining time 1 h), while the UV-radiation exposure is limited to a ~ 50 -ms snapshot for cell illumination and is also minimized by the presence of a 60% neutral density filter. As shown in Fig. 2, the average survival for the control dishes (i.e. plating efficiency) exposed only to a typical scanning procedure is $88.8 \pm 0.7\%$. The $\sim 10\%$ survival reduction observed is mainly due to the low plating efficiency of V79 cells seeded on Mylar film after only 4 h. A minimum of two control dishes are generally used during a single experimental day. These dishes are set up at the same time and following the same protocol used for the irradiated dishes, providing very good estimates of the plating efficiency for each individual experiment.

A second type of control experiment (blank irradiation) was also performed to investigate effects produced by the irradiation of the culture medium. For these experiments, the X-ray beam was deliberately targeted to empty spaces between cells in a normally populated dish for a period equivalent to the delivery of 1 Gy (i.e. $\sim 12,000$ photons). Several studies have reported the potential of medium transferred from irradiated to nonirradiated cells to reduce

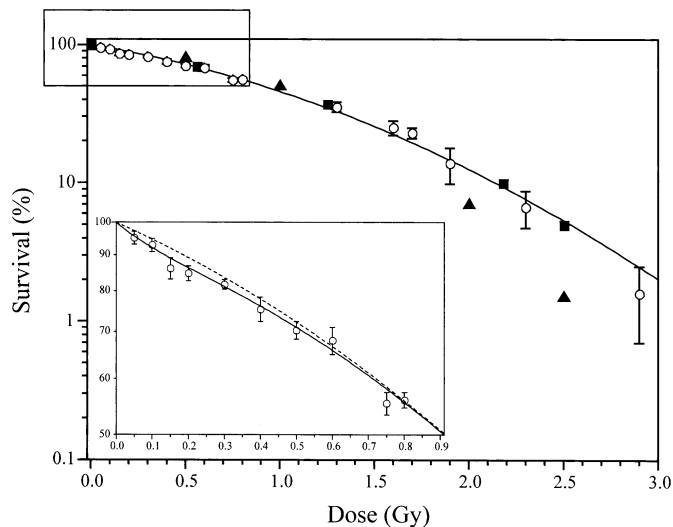


FIG. 3. Survival curve for V79 cells irradiated with a focused beam of C_K X rays (○). Each point is the average of five or more experiments in which ~ 150 cells/experiment were irradiated. Errors are ± 1 SEM. (---) Linear-quadratic fit [$\alpha = (0.52 \pm 0.07) \text{ Gy}^{-1}$, $\beta = (0.26 \pm 0.05) \text{ Gy}^{-2}$]; (—) modified linear-quadratic fit (10) [$\alpha = (0.52 \pm 0.06) \text{ Gy}^{-1}$, $g = (0.9 \pm 0.4)$, $d = (0.19 \pm 0.07) \text{ Gy}$, $\beta = (0.26 \pm 0.05) \text{ Gy}^{-2}$]. (■) From Thacker *et al.* (8) and (▲) from Raju *et al.* (9), both using conventional clonogenic assays and broad-field exposure.

clonogenicity (10). Although our experimental scenario is different (there is no transfer of medium between cell culture dishes), the blank irradiation control experiment is performed to determine if any chemical changes occurring in the medium due to the irradiation have a significant impact on the plating efficiency. As clearly shown in Fig. 2, the average survival for the blank irradiation is $87.8 \pm 0.7\%$, which is in good agreement with the scan-only survival (88.8 ± 0.7), indicating that the irradiation of the medium has no effect on the surviving fraction.

Bystander Data

Initial experiments were designed to reproduce a traditional survival curve by irradiating every cell present in the selected area with a predetermined dose of C_K X rays. The single cell clonogenic assay has already been used successfully in combination with the charged-particle microbeam (9), and it has proven to be particularly sensitive at low doses (< 1 Gy). The data reported in Fig. 3 follow a linear-quadratic trend, in good agreement with published data (12, 13) obtained using broad-field irradiation and conventional clonogenic assays. Although in the microprobe experiments the energy is deposited in a volume of a few μm^3 , spatially and temporally, overlapping of ionizations tracks is very unlikely to occur due to the short tracks of the secondary electrons (7 nm) and the low dose rate (< 2 Gy/s). This may explain the agreement between the microprobe and broad-field experiments in spite of the different energy distribution within the cells. Due to the high sensitivity of the assay at low doses, most of the experimental

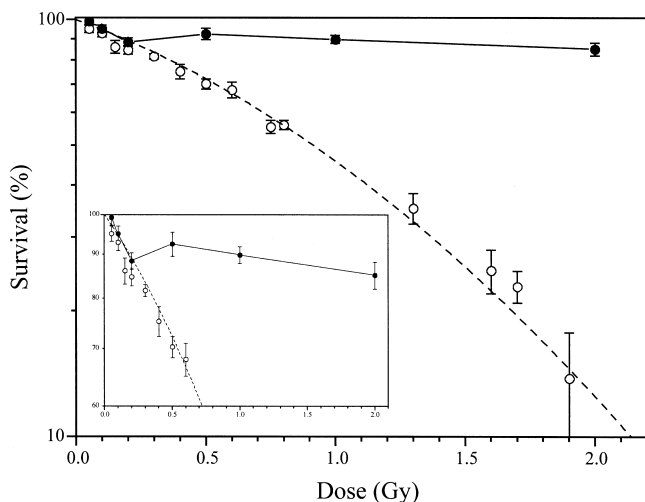


FIG. 4. Comparison of surviving fractions after all-cell irradiation (\circ) and single-cell irradiation (\bullet).

points have been concentrated below 1 Gy, with the cell killing effect of 50 mGy of C_K X rays easily detectable. Statistical analysis reveals a minor but significant discrepancy with the linear-quadratic fit, suggesting that a modified linear-quadratic model, based on inducible repair (14), would describe the experimental data better.

To estimate the extent of the bystander effect, a single cell located approximately in the center of the dish was irradiated with a preselected dose; after the incubation period, the survival of the whole population was assessed by revisiting all the cells. The results are reported in Fig. 4, and they clearly show a bystander effect quantifiable as a $\sim 10\%$ reduction in clonogenic potential. The effect appears to show a dose response below 200 mGy (where there is no significant difference in the surviving fraction after a single-cell and an all-cell irradiation). Above 200 mGy, a constant surviving fraction is observed up to the highest dose considered (2 Gy).

Distance Analysis

Measuring the overall fraction of surviving cells is only the first step in investigating the effect of a single-cell irradiation using the ultrasoft X-ray microprobe. Since the assay is based on the analysis of individual cells, the coordinates of all cells prior to the irradiation are stored in a file together with other details such as progressive cell number, nuclear size, brightness and the eventual dose delivered to that cell. By correlating the fate of each single sample to its position on the dish, spatial analyses can be performed. In particular, the relationship of the distance between the damaged cells and the irradiated cell can be assessed precisely. The whole experimental area of the dish can be divided into a series of virtual circular annuli centered on the irradiated cell. The width of each annulus was set at 500 μm to obtain a statistically relevant number of samples in each annulus, as shown in Fig. 5. The fraction

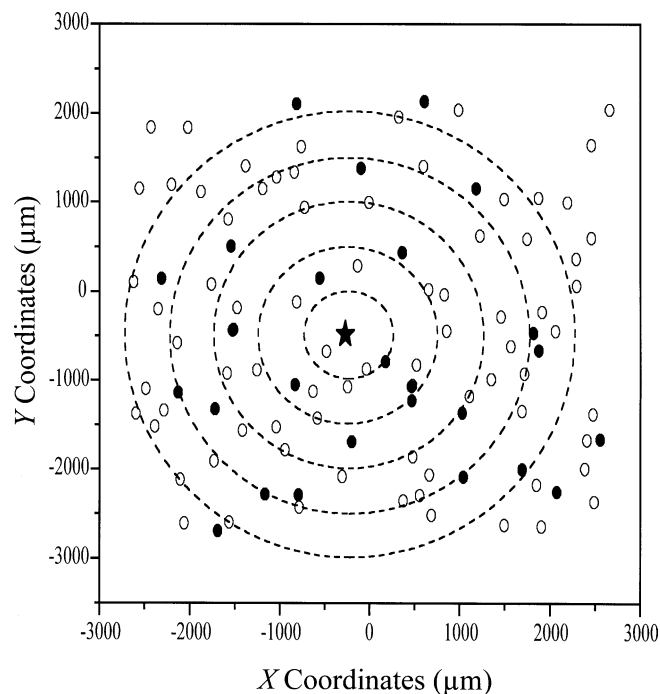


FIG. 5. Example of cell distribution in the microprobe dish. Coordinates of all single cells found prior to the irradiation ($\circ + \bullet$) are plotted as function of their X and Y coordinates. Open circles represent cells that managed to form healthy colonies while filled circles indicate damaged cells. (\star) is the position of the irradiated cell. Dashed lines are for illustrative purposes only.

of damaged cells in each annulus area was then reported as function of the mean distance of the annulus from the irradiated cell (Fig. 6). Since the experiments were performed using a $5 \times 5\text{-mm}^2$ area of the dish, the maximum distance between damaged cells and the irradiated cell was limited to ~ 3 mm. The increased fraction of damaged cells measured in each annulus relative to the control dish was

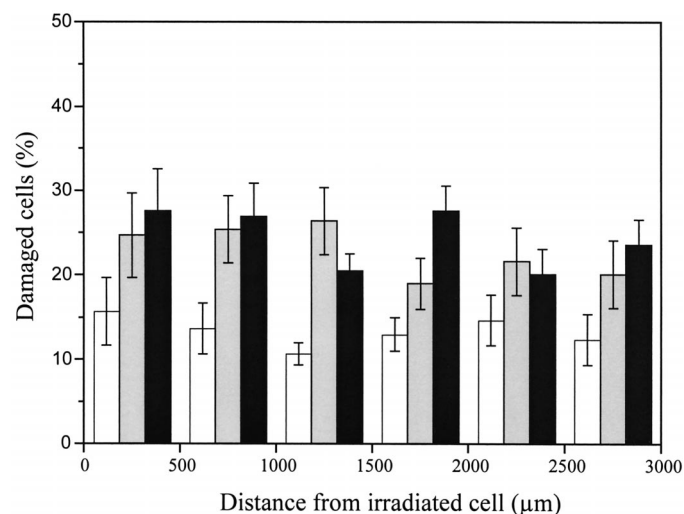


FIG. 6. Fraction of damaged cells as function of distance from the irradiated cell. (\square) Control dishes, (\square) single cell irradiated with 200 mGy, (\blacksquare) single cell irradiated with 2 Gy.

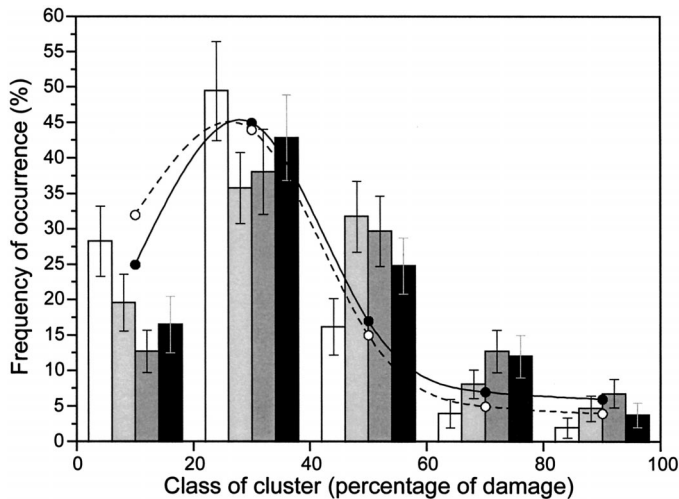


FIG. 7. Frequency of occurrence of clusters of damaged cells as a function of their complexity. (□) Control dishes, (■) single cell irradiated with 100 mGy, (■) single cell irradiated with 200 mGy, (■) single cell irradiated with 2 Gy. The dashed line (---) represents the theoretical simulation for the control dishes, while the solid line (—) indicates the result of the simulation for the irradiated dishes.

a further indication of the bystander effect occurring when an irradiation took place. Furthermore, the fraction of damaged cells per annulus was statistically constant over the distance range considered for each dose examined. This is a clear indication that the distance between the irradiated sample and the damaged cells is not a critical parameter in the bystander effect. Within the considered range of 3 mm, a cell has the same probability of responding to the bystander signal whatever distance it is from the irradiated unit.

Cluster Analysis

Although the distance from the irradiated cells does not appear to play a critical role in the expression of the bystander effect, during the cell scoring, it became evident that the cells that failed to form healthy colonies were not distributed randomly through the dish. By correlating the coordinates of all cells in the dish with their survival outcome, it was possible to check for the presence of clusters of damaged cells. To perform such an analysis, the fraction of locally damaged cells was calculated in the area surrounding each cell ($<500 \mu\text{m}$ radius). The value of $500 \mu\text{m}$ was again chosen since it defined a small area in which, on average, there would be a statistically significant number of cells (~ 6 cells). The frequency with which these clusters appeared is shown in Fig. 7 as a function of cluster complexity (i.e. percentage of damaged cells in the cluster). Areas with between 0 and 20% damaged cells are shown in the first histogram. Areas with between 20 and 40% damaged cells are shown in the second, and so on. The data have also been separated according to the dose delivered to the single irradiated cell.

As expected, the frequency distributions of the occur-

rence of the different types of clusters follow a Poisson distribution. The data in Fig. 7 show a clear shift toward clusters with higher numbers of damaged cells for the irradiated dishes compared to the control. This observed shift cannot be attributed simply to the higher number of damaged cells in the irradiated dishes. Theoretical simulations based on the distribution and number of the initial and damaged cells around the dish were performed and compared with the experimental data (Fig. 7). The simulations also take into account the different fractions of total damaged cells in the control dishes (average 12%) and the irradiated dishes (average 18% when not corrected for the control). As expected, the higher number of damaged samples present in the irradiated dishes shifted the simulated cluster distribution slightly toward clusters with higher numbers of damaged cells. However, this does not fully explain the shift observed with the experimental data. While the simulation for the control is in excellent agreement with the data (i.e. random distribution of damage cells), the data from the irradiated samples indicate a non-random distribution of the damaged cells around the cell dish. No significant difference in the distribution of the clusters was observed as a function of the dose delivered to the single irradiated cell.

DISCUSSION

The bystander effect has generated considerable interest in recent years, and microbeam techniques represent unique tools to investigate it. The Gray Cancer Institute soft X-ray microprobe was therefore used to investigate the extent of the bystander effect on the survival of V79 cells by irradiating a single cell with a focused carbon K-shell X-ray beam. The data reported in this paper show a clear bystander effect that was responsible for the clonogenic death of about 10% of the cells. Typically, under the conditions used here, when a single cell was targeted, an additional 10–15 cells died through a bystander-mediated effect. Since the effect was observed when only a single cell was targeted, it suggests that in this system, every cell has the potential to release a bystander signal. Although the extent of the effect measured in these experiments may differ from that reported by others (2, 14), this is the first bystander study performed by irradiating a single cell and individually revisiting the nonirradiated neighboring cells *in situ*. As a unique feature of these experiments, the cells were not removed from their original position to avoid further stress due to trypsinization and to avoid altering of the distances between cells. This increased the sensitivity for measuring cell killing at low doses. Under conditions where only a single cell was targeted, the effects of 50 mGy were easily detected. Bystander effects have been detected both in systems where cells are in contact (and cell-to-cell communication is plausible) and in those in which considerable distances separate the cells. In our case, single cells were separated by an average distance of $150 \mu\text{m}$ for the duration

of the experiment. The bystander effect appeared to be independent of dose over a large range (up to 2 Gy) with an indication of a dose effect below 200 mGy. This is in contrast to all previously reported measurements of the bystander process that suggest a binary behavior. Comparing the bystander data with the all-cell irradiation data, it also appears that there was no significant difference in the surviving fractions at low doses. Below 200 mGy, the survival potential was dominated by the bystander effect. Only at higher doses did the direct effect of radiation start to play a fundamental role in cell killing, as hypothesized by Brenner *et al.* (15). Interestingly, the dose response detected for the bystander effect indicates the possibility of modulating the extent of the bystander effect with very small doses of radiation. More experiments are planned to test this hypothesis.

In this paper, the analysis of the spatial distribution of damaged and surviving cells is also reported. Since the coordinates of all cells are known, it is possible to map the distribution of damaged cells relative to the irradiated cell or relative to the surviving cells. By plotting the fraction of damaged cells as a function of the distance from the single irradiated cell, we showed that a cell has the same chance of responding to the bystander signals whatever its distance (up to 3 mm) from the irradiated cell. In the case of cells that are not in contact with each other, it is therefore possible to conclude that the bystander signal is still saturated at 3 mm. On the other hand, the distribution of damaged cells in the dish was not random but instead showed a statistically significant clustering effect. Cells that failed to form healthy colonies as a result of a bystander signal were positioned closer to each other than expected from theoretical simulations based on a random sample distribution. This result could also support the hypothesis that cells affected by the bystander signal may themselves release a further signal that triggers a chain reaction. This may be indicative of a cascade reaction, as predicted previously from our studies in human fibroblasts (16, 17). In conclusion, the spatial analysis reveals that the bystander effect is spread over the whole cell culture dish, although not in a uniform way.

ACKNOWLEDGMENTS

This work was supported by the U.S. Department of Energy (DE-FG07-99ER62877, DE-FG02-01ER63236), Cancer Research UK, and the European Community (FIGH-CT1999-00003, FIGH-CT1999-00012). The authors are grateful to Dr. Simon Ameer-Beg for assistance with the two-photon confocal measurements and Dr. Christian David (PSI, Villigen, CH) for the provision of zone plates.

Received: December 18, 2002; accepted: April 28, 2003

REFERENCES

1. M. C. Joiner and H. Johns, Renal damage in the mouse: The response to very small doses per fraction. *Radiat. Res.* **114**, 385–398 (1988).
2. C. B. Seymour and C. Mothersill, Relative contribution of bystander and targeted cell killing to the low-dose region of the radiation dose-response curve. *Radiat. Res.* **153**, 508–511 (2000).
3. B. Marples, P. Lambin, K. A. Skov and M. C. Joiner, Low dose hyper-radiosensitivity and increased radioresistance in mammalian cells. *Int. J. Radiat. Biol.* **71**, 721–735 (1997).
4. M. A. Hill, D. L. Stevens, D. A. Bance and D. T. Goodhead, Biological effectiveness of isolated short electron tracks: V79-4 cell inactivation following low dose-rate irradiation with Al_K ultrasoft X-rays. *Int. J. Radiat. Biol.* **78**, 967–979 (2002).
5. M. Folkard, B. Vojnovic, K. M. Prise, A. G. Bowey, R. J. Locke, G. Schettino and B. D. Michael, A charged-particle microbeam: I. Development of an experimental system for targeting cells individually with counted particles. *Int. J. Radiat. Biol.* **72**, 375–385 (1997).
6. M. Folkard, B. Vojnovic, K. J. Hollis, A. G. Bowey, S. J. Watts, G. Schettino, K. M. Prise and B. D. Michael, A charged-particle microbeam: II. A single-particle micro-collimation and detection system. *Int. J. Radiat. Biol.* **72**, 387–395 (1997).
7. G. Schettino, M. Folkard, B. Vojnovic, A. G. Michette, D. Stekel, S. J. Pfauntsch, K. M. Prise and B. D. Michael, The ultrasoft X-ray microbeam: A sub-cellular probe of radiation response. *Radiat. Res.* **153**, 223–225 (2000).
8. M. Folkard, G. Schettino, B. Vojnovic, S. Gilchrist, A. G. Michette, S. J. Pfauntsch, K. M. Prise and B. D. Michael, A focused ultrasoft X-ray microbeam for targeting cells individually with sub-micrometer accuracy. *Radiat. Res.* **156**, 796–804 (2001).
9. G. Schettino, M. Folkard, K. M. Prise, B. Vojnovic, A. G. Bowey and B. D. Michael, Low-dose hypersensitivity in Chinese hamster V79 cells targeted with counted protons using a charged-particle microbeam. *Radiat. Res.* **156**, 526–534 (2001).
10. C. Mothersill and C. Seymour, Medium from irradiated human epithelial cells but not human fibroblasts reduces the clonogenic survival of unirradiated cells. *Int. J. Radiat. Biol.* **71**, 421–427 (1997).
11. J. Thacker, R. E. Wilkinson and D. T. Goodhead, The induction of chromosome exchange aberrations by carbon ultrasoft X-rays in V79 hamster cells. *Int. J. Radiat. Biol.* **49**, 645–656 (1986).
12. M. R. Raju, S. G. Carpenter, J. J. Chmielewski, M. E. Schillaci, M. E. Wilder, J. P. Freyer, N. F. Johnson, P. L. Schor, R. J. Serbing and D. T. Goodhead, Radiobiology of ultrasoft X-rays I. Cultured hamster cells (V79). *Radiat. Res.* **110**, 396–412 (1987).
13. M. C. Joiner and H. Johns, Renal damage in the mouse: The response to very small doses per fraction. *Radiat. Res.* **114**, 385–398 (1988).
14. S. G. Sawant, G. Randers-Pehrson, N. F. Metting and E. J. Hall, Adaptive response and the bystander effect induced by radiation in C3H 10T_{1/2} cells in culture. *Radiat. Res.* **156**, 177–180 (2001).
15. D. J. Brenner, J. B. Little and R. K. Sachs, The bystander effect in radiation oncogenesis: II A quantitative model. *Radiat. Res.* **155**, 402–408 (2001).
16. K. M. Prise, O. V. Belyakov, M. Folkard and B. D. Michael, Studies of bystander effects in human fibroblasts using a charged particle microbeam. *Int. J. Radiat. Biol.* **74**, 793–798 (1998).
17. O. V. Belyakov, A. M. Malcolmson, M. Folkard, K. M. Prise and B. D. Michael, Direct evidence for a bystander effect of ionizing radiation in primary human fibroblasts. *Br. J. Cancer* **84**, 674–679 (2001).